Optics Letters

Quantitative blood oxygen saturation imaging using combined photoacoustics and acousto-optics

Altaf Hussain,* Wilma Petersen, Jacob Staley, Erwin Hondebrink, and Wiendelt Steenbergen

Biomedical Photonic Imaging group, MIRA Institute for Biomedical Technology and Technical Medicine, University of Twente, P.O. Box 217, 7500 AE Enschede, The Netherlands
**Corresponding author: a.hussain@utwente.nl*

Received 24 November 2015; revised 19 February 2016; accepted 3 March 2016; posted 4 March 2016 (Doc. ID 254355); published 5 April 2016

In photoacoustic spectroscopy (PAS), wavelength dependent optical attenuation of biological tissue presents a challenge to measure the absolute oxygen saturation of hemoglobin (sO_2). Here, we employ the combination of photoacoustics and acousto-optics (AO) at two optical wavelengths to achieve quantification, where AO serves as a sensor for the relative local fluence. We demonstrate that our method enables compensation of spatial as well as wavelength dependent fluence variations in PAS without *a priori* knowledge about the optical properties of the medium. The fluence compensated photoacoustic images at two excitation wavelengths are used to estimate the absolute oxygen saturation of blood in a spatially and spectroscopically heterogeneous phantom.

OCIS codes: (170.3880) Medical and biological imaging; (110.0113) Imaging through turbid media; (170.5120) Photoacoustic imaging; (170.1470) Blood or tissue constituent monitoring; (170.2655) Functional monitoring and imaging; (170.1065) Acousto-optics.

http://dx.doi.org/10.1364/OL.41.001720

Photoacoustic (PA) imaging has emerged as a promising biomedical imaging modality. It benefits from the rich optical contrast of biological tissue and ultrasonic resolution. Its applications include preclinical studies of tumor progression, breast imaging, imaging of microvasculature, and small animal imaging [1–3]. A major challenge is that PA images do not quantify the local optical absorption of the tissue. Instead, in PA imaging, the reconstructed images of initial stress distribution σ_o are proportional to absorbed optical energy density E_a,

$$\sigma_o = \Gamma E_a = \Gamma \mu_a \varphi, \tag{1}$$

where μ_a is the optical absorption coefficient, the desired tissue parameter, and ϕ is the unknown local fluence. The problem of knowing the exact fluence, or variation in the fluence due to change in excitation wavelength, is challenging because of its dependence on optical properties of the background tissue. As a result, the entanglement of μ_a and ϕ in Eq. (1) restricts the use of PA to qualitative imaging. Eliminating the dependency on ϕ from PA imaging will enable quantitative PA spectroscopy (PAS)—a potential tool for deep tissue molecular and functional imaging [4].

One important example of functional imaging is the estimation of absolute blood oxygen saturation (sO_2) at the vasculature level. The blood sO_2 level provides information about the healing of wounds [5,6], response to chemo and radio therapy during tumor treatment, and oxygenation heterogeneity in tumors [7,8]. Measuring blood sO_2 based on PAS alone [9,10], relies on assumptions that have limited scope in realistic situations. Previously, we have demonstrated an experimental technique to compensate PA signals for fluence variations [11]. The technique relates the signals of two PA measurements and an acousto-optic (AO) measurement to the local absorption coefficient $\mu_{a,2}$ at point 2 inside the turbid media,

$$\mu_{a,2} = \kappa \sqrt{\frac{p^*_{1,2} p^*_{3,2}}{P^*_{l,123}}}, \tag{2}$$

where $p^*_{1,2}$ and $p^*_{3,2}$ are normalized PA signals originating at internal point 2 by exciting the medium sequentially at surface points 1 and 3, $P^*_{l,123}$ is the normalized AO signal, being the power of tagged light measured at point 3 when the medium is excited at point 1 and ultrasound (US) focus is placed at point 2, and κ is an instrumental constant. Details about involved parameters can be found in [11].

In this Letter, we demonstrate the technique's potential to do functional imaging of tissue. The proposed method to measure sO_2 is potentially advantageous to the previously reported method based on PAS alone because it does not rely on any assumption regarding light attenuation properties of the tissue or light transport model; instead the dependence on optical properties is eliminated through an additional AO experiment. We make use of the AO assisted fluence compensated PA measurements at two optical wavelengths to estimate the absolute sO_2 of blood. We performed measurements on whole human blood with varying levels of sO_2 circulating in a tube imbedded in an optically heterogeneous tissue phantom and validated our results against measurements with a blood oximeter.

In Eq. (2), the local μ_a is expressed in terms of experimentally measurable quantities only, unlike in Eq. (1) where the unknown local ϕ is part of the problem. In Eq. (2), $P^*_{l,123}$ is the power of ultrasonically tagged light which can be measured in an absolute manner using the interferometric detection principle. However, if AO measurements are performed using a speckle contrast (C) based detection method, as we have done here, one measures the change in speckle contrast (ΔC) between the on and off states of US. In a typical AO experiment, where short bursts of high frequency (>1 MHz) US are used to tag the light in a diffused background, the ΔC is proportional to the power of the ultrasonically tagged light $P^*_{l,123}$ [12]. The change in the contrast depends on the AO properties of the insonified region [13]:

$$\Delta C \cong \bar{s}\left(n_o k_o \frac{P_o}{\rho v_a^2}\right)^2 \eta^2 \frac{v_a}{f_a}, \tag{3}$$

where $\bar{s}$ is the optical mean path length within the US focus for a given light propagation geometry, n_o is the refractive index, $k_o = 2\pi/\lambda$ is the wave number, P_o and f_a are the pressure and frequency of the applied US, ρ is the medium density, v_a is the speed of sound, and η is the elasto-optic coefficients which are properties of the tissue within the US focus. During multiple optical wavelength AO measurements, all the acoustic parameters in Eq. (3) remain the same. Considering the changes in $\bar{s}$ and n_o within the US focus volume, to be negligible for used optical wavelengths, Eq. (3) implies that the measured ΔC needs to be normalized by the square of optical wave number k_o to account for its dependence on the optical wavelength. Hence, the power of ultrasonically tagged light at a given optical wavelength in terms of speckle contrast change is expressed as $P^*_{l,123} \propto \lambda^2 \Delta C(\lambda)$. Now we rewrite Eq. (2) in terms of ΔC as

$$\mu_{a,2}(\lambda) = \kappa \sqrt{\frac{p^*_{1,2}(\lambda) p^*_{3,2}(\lambda)}{\lambda^2 \Delta C(\lambda)}} = \kappa M(\lambda), \tag{4}$$

where M is the AO assisted fluence compensated PA image value.

In whole human blood, oxygenated (HbO_2) and deoxygenated (Hb) hemoglobin are the two dominant chromophores responsible for optical absorption in the near infrared spectral region, therefore, the absorption coefficient can be written as

$$\mu_a(\lambda) = c_{HbO_2} \epsilon_{HbO_2}(\lambda) + c_{Hb} \epsilon(\lambda_{Hb}), \tag{5}$$

where c_{HbO_2} and c_{Hb} are the concentrations of HbO_2 and Hb, respectively, and ϵ_{HbO_2} and ϵ_{Hb} are the corresponding molar extinction coefficients. In order to measure c_{HbO_2} relative to the total concentration $c_T = c_{HbO_2} + c_{Hb}$ of blood, one needs to evaluate Eq. (4) at two excitation wavelengths. Rewriting Eq. (4) using Eq. (5) in terms of c_{HbO_2} and c_T for excitation wavelengths $\lambda 1$ and $\lambda 2$ leads to

$$c_{HbO_2} \Delta \epsilon_{\lambda 1} + c_T \epsilon_{Hb,\lambda 1} = \kappa M_{\lambda 1}, \tag{6}$$

$$c_{HbO_2} \Delta \epsilon_{\lambda 2} + c_T \epsilon_{Hb,\lambda 2} = \kappa M_{\lambda 2}, \tag{7}$$

where $\Delta\epsilon = \epsilon_{HbO_2} - \epsilon_{Hb}$. Assuming κ is independent of wavelength and solving Eqs. (6) and (7) together for the fraction of oxygenated blood $sO_2 = c_{HbO_2}/c_T$ results in

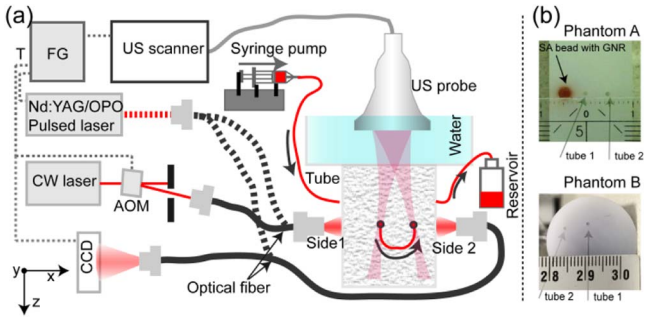

Fig. 1. (a) Schematic of the combined experimental setup for PA and AO for measuring blood sO_2. AOM, acousto-optic modulator; T, trigger signal for synchronization of lasers and CCD camera; US scanner, MyLab One (a portable US machine). (b) Photo of the phantoms used, cross section of the image plane made after the measurement. SA, sodium alginate; GNR, gold nanorods.

$$sO_2 = \frac{M_{\lambda 1}\epsilon_{Hb,\lambda 2} - M_{\lambda 2}\epsilon_{Hb,\lambda 1}}{M_{\lambda 2}\Delta\epsilon_{\lambda 1} - M_{\lambda 1}\Delta\epsilon_{\lambda 2}}. \tag{8}$$

Here, all the parameters are either known from the spectrum of the blood or experimentally measurable.

The schematic of the combined experimental setup for PA and AO is depicted in Fig. 1(a). For PA measurements, a tunable optical parametric oscillator (OPO, Spectra Physics VersaScan-L) pumped by a frequency-doubled Q-switched Nd:YAG laser (Newport QuantaRay lab series 170) delivering 6 ns pulses was used. The light is delivered from the laser to the sample with optical fiber bundles from side 1 and side 2, sequentially. The pulse energy used was between 2 mJ and 3 mJ with an illumination spot of 8 mm diameter. A clinical US scanner (MyLab One, ESAOTE Europe) connected to a 64 channel (effective aperture of 15.7 mm) linear US probe (SL3332, ESAOTE) is used for the detection of PA signals while transmission of US was turned off. The US probe has a central frequency of 4.3 MHz and a bandwidth of 120% at −6 dB. Radio frequency (RF) signals acquired by the US scanner were saved to the computer and image reconstruction was performed offline using Fourier reconstruction [14]. The reconstructed 2D images are of the cross-sectional plane (x–z plane).

AO measurements were performed using the parallel speckle detection method. The laser beam from a tunable continuous wave (CW) laser (Coherent MBR EL Ti:Sapphire, pumped by a single mode 532 nm laser Coherent Verdi 6) was chopped into pulses of 1 μs at a repetition rate of 10 kHz using an AO modulator (AOM) triggered by the US machine. The light was delivered with an optical fiber bundle from the output of the AOM to the sample from side 1. US bursts consisting of five cycles at a center frequency of 5 MHz were transmitted for modulation of light using 64 channels of the linear US probe. Synthetic focusing was implemented by introducing time delays between transmitted signals in order to achieve the desired focusing depth and steering angle. The delays between the US burst and the laser pulse were set using a function generator, which allowed the US to propagate (along the z axis, Fig. 1) configurable distances before interrogating the region of interest with light. Ultrasonically modulated light was collected from side 2 with an optical fiber bundle and detected by a charge-coupled device (CCD) camera as depicted in Fig. 1(a).

We performed experiments on two tissue phantoms, namely, phantom A and phantom B, shown in Fig. 1(b). The bulk of both phantoms were prepared by mixing 8% (v/v) of 20% Intralipid (Sigma Aldrich) and 3% (w/v) of agar (Sigma Aldrich) in water. This mixture resulted in a reduced scattering coefficient (μ_s') of approximately 8.7, 8.9, 9.2, and 9.3 cm^{-1} at used wavelengths of 750, 755, 780, and 800 nm, respectively. Homogeneous background absorption was introduced by mixing 2 μl black ink (Ecoline, Royal Talens) in 100 ml of solution in phantom A and 15 μl in 100 ml of solution in phantom B. Inhomogeneity in optical properties in phantom A was introduced by embedding a strongly absorbing ($\mu_a = 4.2$ mm^{-1} at 755 nm and $\mu_a = 5.11$ mm^{-1} at 780 nm) sodium alginate (SA) bead containing gold nanorods (GRNs). A nylon tube (inner and outer diameter of 0.56 and 0.96 mm) passing through the phantoms at two depths under the surface was used to mimic two blood vessels. Blood samples were obtained from two anonymous healthy volunteers organized by the donor service at the Experimental Centre of Technical Medicine at the University of Twente.

Blood samples with sO_2 between 5% and 93% were used for measurements. Different values of sO_2 were obtained by adding sodium dithionite ($Na_2S_2O_4$) to the whole blood. A syringe pump placed on a motorized stage that was constantly tilted to avoid red blood cell sedimentation was used to pump the blood through the tube. Oxygen saturation values of the blood samples were measured using a blood oximeter (Avoximeter 1000E, ITC point of care) before and after each experiment for comparison with photoacoustically estimated sO_2.

Figure 2 shows an example of fluence compensation of PA images using Eq. (4), at two wavelengths $\lambda = 755$ nm and $\lambda = 780$ nm in phantom A, for blood at a 5% oxygen saturation. First, two PA measurements were performed at each wavelength by exciting the phantom from side 1 and side 2 [see Fig. 1(a)]. Figures 2(a)–2(d) show the acquired PA images of the photographed plane of the phantom shown in Fig. 1(b). In these images, only the top and bottom surfaces of the three absorbers are reconstructed; this is due to the limited bandwidth and limited view of the linear array (nominal bandwidth 2.5–7.5 MHz). Then, AO measurements were performed such that the optodes coincide with the PA excitation points and the US focus interrogates the region of interest (ROI), where fluence compensation is required. Figure 2(e) shows the AO signal: the measured ΔC as function of US burst position along the lines in the x–z plane that pass from the probe through tube 1 and tube 2 [see Fig. 1(a)]. Each measurement point is an average of ten measurements in order to improve signal to noise ratio. The ΔC is expected to show a maximum at $z \cong 34$ mm, where the US focus coincides with the illumination and optical detection plane. Local minima in ΔC at $z \cong 33$ mm are caused by the blood filled tubes. By using two PA images and values of ΔC at the location of blood filled tubes in Eq. (4), we get the fluence compensated PA images at each wavelength. Figures 2(f) and 2(g) show the fluence compensated PA images at $\lambda = 755$ nm and $\lambda = 780$ nm, respectively.

Figure 3 shows the line profiles along the x axis of the PA images in Fig. 2 to give a quantitative impression of the variations in PA image values before and after the fluence compensation. Figure 3(a) corresponds to images before the fluence compensation, where the image values from two optically identical tubes are different due to the variations in

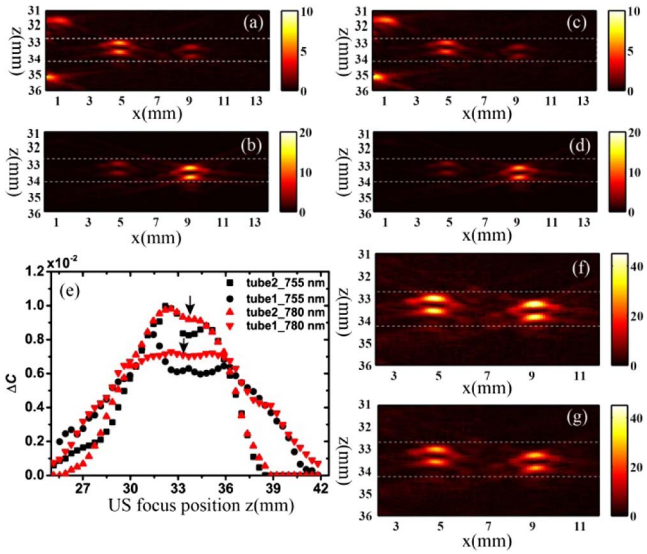

Fig. 2. Example of fluence compensation of PA images of 5% oxygenated blood sample at $\lambda = 755$ nm and $\lambda = 780$ nm in phantom A. (a) and (b) PA images acquired at $\lambda = 755$ nm; (a) by exciting the medium from side 1 and (b) by exciting the phantom from side 2. (c) and (d) PA images acquired at $\lambda = 780$ nm; (c) by exciting medium from side 1 and (d) by exciting phantom from side 2. (e) Measured ΔC as US focus propagates along a line in the x–z plane through the tubes containing blood at $\lambda = 755$ nm and $\lambda = 780$ nm. Black arrows indicate tube positions as obtained from PA images; (f) and (g) fluence compensated PA images at $\lambda = 755$ nm and $\lambda = 780$ nm.

fluence. The effect of the strongly absorbing SA bead is reflected in Figs. 2(a) and 2(c), where the phantom is excited from side 1 and the bead causes a shadow on both of the tubes resulting in lower image values. Further, the ratio of PA image values from tube 1 to tube 2 varies depending on the excitation wavelength and illumination point due to the wavelength-dependent optical attenuation of the background. Figure 3(b) corresponds to the AO assisted fluence compensated PA images. In this case, the PA image values from both tubes are equal and directly relate to the optical absorption of the target. Further, the ratio of 1.40 of the fluence compensated PA signals from both tubes at $\lambda = 755$ nm to $\lambda = 780$ nm is in agreement with the known absorption spectrum of the 5% oxygenated blood [15].

We measured sO_2 of whole human blood samples while the blood was pumped through the tube embedded in the phantoms. For each blood sample, we obtained fluence compensated PA images at two wavelengths, 755 and 780 nm in phantom A, following the procedure described above. The

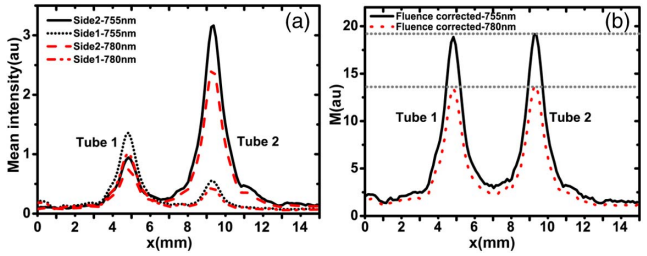

Fig. 3. Comparison of the PA image value (a) before and (b) after fluence compensation at $\lambda = 755$ nm and $\lambda = 780$ nm.

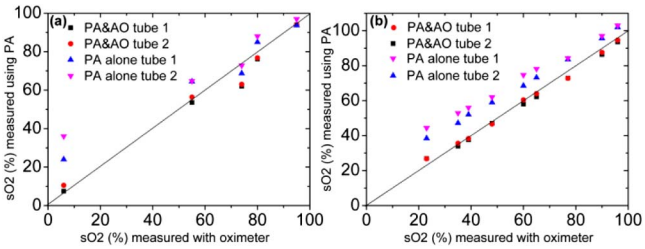

Fig. 4. Comparison of the estimated sO_2 using PA alone and AO assisted fluence compensated PA versus sO_2 measured with an oximeter; solid line represents the perfect estimation. (a) Results for phantom A and (b) results for phantom B. The legend PA&AO refers to the sO_2 estimation based on the AO assisted fluence compensated PA measurements.

volume integrated fluence compensated PA values (M) from each tube at both wavelengths (with an equal number of pixels included from each target) are used in Eq. (8) to estimate the sO_2. For comparison, we estimated the sO_2 using the PA measurements at two wavelengths without the fluence compensation. For this estimation, we considered the images acquired by illuminating the medium from one side [side 1, see Fig. 1(a)].

Figure 4(a) shows the estimated sO_2 values of five blood samples in phantom A, using PA alone and AO assisted fluence compensated PA, and are plotted against sO_2 values measured with the oximeter. The estimation of sO_2 based on PA alone resulted in the positive bias in both tubes compared to measurements using the oximeter, and the bias is higher for the tube located further away from the excitation point. This bias is a result of the variation in the local fluence with the excitation wavelength; in comparison, the estimation of the sO_2 values based on the AO assisted fluence compensated PA (PA&AO) is in good agreement with the measurements using the oximeter, regardless of the depth of the tube inside the phantom. However, the sample with an actual oxygenation of 74% presents a relatively large error. Since this result deviates from the expected range both before and after the fluence compensation, the error could be experimental and caused by the blood sedimentation in the syringe.

To eliminate this error, we decreased the measurement time by automatizing the wavelength tuning and excitation pulse energy measurements in our setup. With the measurement time shorter than the blood sedimentation time in the tube, we repeated the sO_2 measurements for nine blood samples with varying sO_2 values in phantom B. The measurements in phantom B are done using the same method as described above in the case of phantom A, except that the used excitation wavelengths are 750 and 800 nm. Figure 4(b) shows the results of the sO_2 measurements in phantom B, where the estimation of sO_2 based on PA alone and AO assisted fluence compensated PA is plotted against the sO_2 measured with the oximeter. Figure 4(b) shows that the estimation of the sO_2 values using AO assisted fluence compensated PA is, overall, in good agreement with the sO_2 values measured using the oximeter, for all the blood samples for both tubes regardless of their position. Whereas, estimation based on PA alone shows positive bias for both tubes and the bias is position dependent.

Fluence variations due to wavelength dependent optical attenuation of tissue have been the major challenge in achieving quantitative PAS. Our results show that these fluence variations in PAS can be compensated by combining PA with AO spectroscopy, using Eq. (4). We showed that this combination applied at two wavelengths provides an absolute measurement of oxygen saturation of blood without using prior knowledge on the medium's bulk properties. The multiplication factor λ^2 applied on the AO ΔC in Eq. (4) is to account for the wavelength dependency of the light modulation efficiency of theUS. For simplicity, we assumed that the change in the modulation efficiency due to the change in wavelength dependent scattering is negligible. In our previous work, we have shown that the changes in light modulation efficiency of the US due to changes in local scattering are negligible within a biological relevant range of scattering levels [16]. The assumption is, further, justified for the used wavelengths from our results in Fig. 4, where we used two different sets of wavelengths 755 and 780 nm in phantom A and 750 and 800 nm in phantom B. The dependence of the modulation efficiency on scattering would have led to a systematic bias in the estimation of oxygen saturation. Nevertheless, it is the validity of this assumption that defines the range of excitation wavelengths for which the method can accurately compensate for wavelength dependent fluence variations and facilitate quantitative PAS. The dependence of the modulation efficiency on the US pressure, US wavelength, and local acoustic properties of the medium will not be the limiting factor, since these either remain constant or can be controlled during multi-wavelength AO measurements.

Future work will focus on translating our approach of measuring absolute sO_2 *in vivo* by using a coherent nanosecond pulsed laser for AO measurements [17], which enables AO measurement orders of magnitude < 100 ns faster than tissue decorrelation time.

Funding. Stichting voor de Technische Wetenschappen (STW) (vici-grant 10831).

REFERENCES

1. P. Beard, Interface Focus **1**, 602 (2011).
2. S. Mallidi, G. P. Luke, and S. Emelianov, Trends Biotechnol. **29**, 213 (2011).
3. L. H. V. Wang and S. Hu, Science **335**, 1458 (2012).
4. B. Cox, J. G. Laufer, S. R. Arridge, and P. C. Beard, J. Biomed. Opt. **17**, 061202 (2012).
5. T. Seki, M. Fujioka, H. Fukushima, H. Matsumori, N. Maegawa, K. Norimoto, and K. Okuchi, Int. J. Burns Trauma **4**, 40 (2014).
6. C. K. Sen, Wound Repair Regen. **17**, 1 (2009).
7. B. J. Moeller, R. A. Richardson, and M. W. Dewhirst, Cancer Metast. Rev. **26**, 241 (2007).
8. P. Vaupel and A. Mayer, Cancer Metast. Rev. **26**, 225 (2007).
9. R. O. Esenaliev, I. V. Larina, K. V. Larin, D. J. Deyo, M. Motamedi, and D. S. Prough, Appl. Opt. **41**, 4722 (2002).
10. J. Xia, A. Danielli, Y. Liu, L. D. Wang, K. Maslov, and L. V. Wang, Opt. Lett. **38**, 2800 (2013).
11. K. Daoudi, A. Hussain, E. Hondebrink, and W. Steenbergen, Opt. Express **20**, 14117 (2012).
12. J. Li, G. Ku, and L. H. V. Wang, Appl. Opt. **41**, 6030 (2002).
13. R. Zemp, S. Sakadzic, and L. V. Wang, Phys. Rev. E **73**, 061920 (2006).
14. M. Jaeger, S. Schupbach, A. Gertsch, M. Kitz, and M. Frenz, Inverse Probl. **23**, S51 (2007).
15. N. Bosschaart, G. J. Edelman, M. C. G. Aalders, T. G. van Leeuwen, and D. J. Faber, Laser Med. Sci. **29**, 453 (2014).
16. A. Hussain, K. Daoudi, E. Hondebrink, and W. Steenbergen, J. Biomed. Opt. **19**, 066002 (2014).
17. S. Resink, E. Hondebrink, and W. Steenbergen, Opt. Lett. **39**, 6486 (2014).